PRAMANA
— journal of
physics

Vol. 56, Nos 2 & 3
Feb. & Mar. 2001
pp. 287–303

Observing SU(2) phases with neutrons

VEER CHAND RAKHECHA* and APOORVA G WAGH†
Solid State Physics Division, Bhabha Atomic Research Centre, Mumbai 400 085, India
Email: *vcr@apsara.barc.ernet.in; †nintsspd@magnum.barc.ernet.in

Abstract. We present an overview of polarized neutron experiments observing SU(2) phases. The first experimental separation of geometric and dynamical phases, the explicit verification of Pauli anticommutation and the first observation of interference amplitudes and phases in noncyclic evolutions are described. These experiments elucidate the physics of phases and phase jumps propounded by the Pancharatnam connection.

Keywords. Spinor; SU(2) phase; Pancharatnam phase; geometric phase; dynamical phase; noncyclic phase; neutron interferometry; neutron polarimetry.

PACS Nos 03.65 Bz; 03.75 Dg; 42.25.Hz; 42.25.Ja

1. Introduction

Neutron, due to its electric neutrality and finite magnetic moment, is an ideal probe of SU(2) phases acquired in cyclic and noncyclic special unitary evolutions. A neutronic experiment [1,2] has clearly demarcated geometric and dynamical phases. The two phase components here arise from distinct physical operations, viz. rotation and translation respectively between two identical neutron spin flippers. This experiment also explicitly verified Pauli anticommutation by reversing a sequence of successive π-precessions about two orthogonal axes. The first observation [3] of interference amplitudes and phases in noncyclic evolutions has clearly brought out the full implications of the Pancharatnam connection.

2. Spinning neutron and SU(2) phases

Neutron is a chargeless spin 1/2 particle with a finite magnetic moment. In a magnetic induction $\mathbf{B}$, the spin-dependent interaction Hamiltonian $-\mu\boldsymbol{\sigma}\cdot\mathbf{B}$ causes an evolution of the 2-component neutron wavefunction Ψ in the 2-dimensional complex Hilbert space. Here μ is the neutron magnetic moment ($-1.913\ \mu_N$) and $\boldsymbol{\sigma}$ is the vector of Pauli spin operators. The general ordered evolution operator $\mathrm{P}\mathrm{e}^{-i\int(-\mu\boldsymbol{\sigma}\cdot\mathbf{B})\mathrm{d}t/\hbar}$, generates an SU(2) phase for the spinor Ψ. In general there is also a spin-independent term in the neutron Hamiltonian due, for instance, to the nuclear interaction with the medium traversed. This produces a scalar, i.e. U(1), phase.

A normalized ray ψ in the ray space, viz.

$$\psi = \cos\frac{\theta}{2}|z\rangle + \sin\frac{\theta}{2}\exp(i\phi)|-z\rangle, \tag{1}$$

differs from the wavefunction Ψ merely by a complex multiplicative factor which strips Ψ of its magnitude and phase information. The corresponding pure state density operator ρ equals $\Psi\Psi^\dagger/\Psi^\dagger\Psi = \psi\psi^\dagger$. In eq. (1), the two base states $|z\rangle$ and $|-z\rangle$ are eigenstates of the z-component σ_z of $\boldsymbol{\sigma}$. The angles θ and ϕ denote the polar coordinates of the unit spin vector $\mathbf{s} = \mathrm{Tr}\rho\boldsymbol{\sigma}$. There is a one-to-one correspondence between the gauge-invariant ray space quantities ρ and $\mathbf{s}$. The Schrödinger evolution of Ψ generates the classical Larmor precession [4] of spin $\mathbf{s}$ at an angular precession frequency $\omega_L = -2\mu B/\hbar$ about the instantaneous magnetic field.

The spin vector $\mathbf{s}$ specifies a ray (1) completely. The spin sphere, i.e. the unit sphere of spin directions, thus constitutes the ray space (or the projective Hilbert space) for the spinor. As Ψ evolves, the tip of $\mathbf{s}$ traces a curve C from $\mathbf{s}_i$ to $\mathbf{s}_f$, say, in the ray space.

The evolution is termed cyclic if C is closed, i.e. $\mathbf{s}_f = \mathbf{s}_i$ and noncyclic [5] if C is open, i.e. $\mathbf{s}_f \neq \mathbf{s}_i$. For a general noncyclic evolution, the Pancharatnam connection [6–8] provides a rigorous definition of phase Φ of the final wavefunction Ψ_f with respect to the initial wavefunction Ψ_i and the associated amplitude of interference $\mathcal{A}$ as

$$\Phi = \arg(\Psi_i^\dagger\Psi_f) \tag{2}$$

and

$$\mathcal{A} = \frac{\left|\Psi_i^\dagger\Psi_f\right|}{\Psi_i^\dagger\Psi_i}. \tag{3}$$

The total phase Φ has a dynamical phase component [9,10]

$$\Phi_D = -\int\frac{\langle-\mu\boldsymbol{\sigma}\cdot\mathbf{B}\rangle\mathrm{d}t}{\hbar} = \int\frac{\mu\mathbf{s}\cdot\mathbf{B}\mathrm{d}t}{\hbar} \tag{4}$$

and a geometric phase component [9,10]

$$\Phi_G = \Phi - \Phi_D = -\frac{\Omega}{2}\,, \tag{5}$$

where Ω is the solid angle subtended at the centre of the spin sphere by the spin trajectory C, closed by the shorter geodesic if the evolution is noncyclic.

Geometric phase depends only on the geometry of the curve traced in the ray space. It is the nonintegrable [6,9], Hamiltonian-independent phase component, equal to the phase anholonomy [11,12] of a parallel transported wavefunction. For a 2-state, this phase anholonomy equals minus half the angle anholonomy for a vector parallel transported along the curve C. Already included in the standard formulation of quantum mechanics, geometric phase arises in completely general [13] evolutions, whether nonadiabatic, noncyclic or even nonunitary. Geometric phase manifests itself in a vast multitude of physical phenomena [14,15].

3. Observation of cyclic SU(2) phases

There are two well-known strategies to observe SU(2) phases. In the first, viz. '2-Hamiltonian 1-state' strategy [15], the phases are determined interferometrically. In the other, the '1-Hamiltonian 2-state' strategy [16–19], a coherent superposition of two orthogonal states, $|z\rangle$ and $|-z\rangle$, say, is subjected to a single Hamiltonian. For a cyclic evolution of $|z\rangle$ state, the $|z\rangle$ and $|-z\rangle$ states acquire equal and opposite SU(2) phases Φ and $-\Phi$ respectively. The final spin of the superposition differs from the initial spin by a rotation -2Φ about $\hat{\mathbf{z}}$. The spinor phase for $|z\rangle$ is inferred polarimetrically from the spin rotation of the superposition.

4. Interferometric observation of separated geometric and dynamical phases

A perfect crystal interferometer was first operated for neutrons a quarter century ago [20]. The neutron interferometer, affording observation of interference between neutron subwaves separated by a few cm over a few cm, has since served as a touchstone for several quantum physical [21,22] concepts.

To observe the spinor phase dependence on the *orientation* of the precession axis, Wagh proposed the interferometric experiment [4] depicted schematically in figure 1. Subsequently, Wagh and Rakhecha showed [10] that the proposed experiment was the first to clearly demarcate geometric and dynamical phases. Here a $|z\rangle$-polarized neutron beam of velocity v incident on the interferometer permeated by a uniform vertical magnetic field $B_0\hat{\mathbf{z}}$, splits into subbeams **1** and **2**. The subbeams are taken to the state $|-z\rangle$ by identical spin flippers F_1 and F_2. The spinor evolution is hence cyclic over path **1** followed by reversed path **2**. For a relative rotation $\delta\beta$ between F_1 and F_2 about $\hat{\mathbf{z}}$, the spin curves traced on paths **1** and **2** enclose [10] a solid angle $\Omega = -2\delta\beta$ of an 'orange slice' on the spin sphere, yielding a pure geometric phase (cf. eq. (5))

$$\Phi_G = -\frac{\Omega}{2} = \delta\beta\,. \tag{6}$$

Thus Φ_G is given by just the *angle* $\delta\beta$ regardless of the Hamiltonian. The phase Φ_G identifies with the phase jump caused by the kink $\delta\beta$ in the spin curve [12,23] at the pole $|-z\rangle$, i.e. at the ray on the 2-sphere orthogonal to the initial ray $|z\rangle$.

A linear translation δx of F_1, say, along its subbeam, leaves the spin curve and hence Φ_G unaltered. However, it changes precessions about the guide field in the $|z\rangle$ and $|-z\rangle$ states by $\delta\phi$ and $-\delta\phi$ respectively on path **1**, to generate a pure dynamical phase shift [10] (cf. eq. (4))

$$\Phi_D = -\delta\phi = -\frac{2|\mu|B_0\delta x}{\hbar v}\,. \tag{7}$$

A translation of F_2 produces an identical dynamical phase, but of opposite sign. As opposed to the geometric phase (cf. eq. (6)), the dynamical phase Φ_D depends on the field B_0 in the Hamiltonian. In this experiment geometric and dynamical phases arise from two distinct physical operations, rotation and translation respectively, of the spin flippers and get separated.

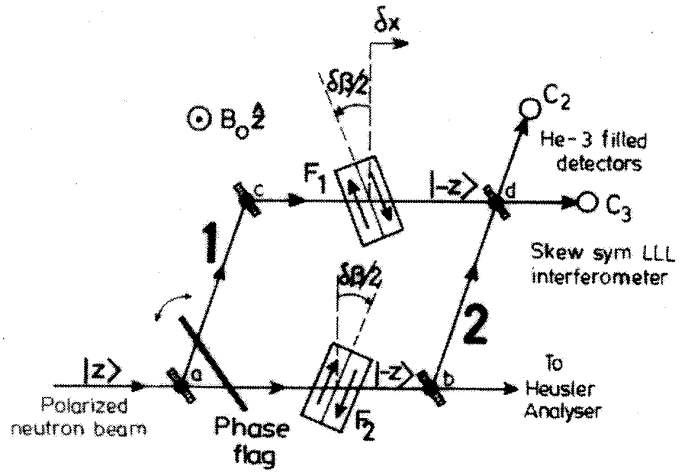

Figure 1. Interferometric separation of geometric and dynamical phases. A relative rotation $\delta\beta$ between the identical π-flippers F_1 and F_2 produces a pure geometric phase Φ_G, equal to $\delta\beta$, for the incident $|z\rangle$-state; their relative translation δx results in a pure dynamical phase Φ_D, proportional to δx. These phases are determined from the shifts of the interferograms generated by rotating the phase flag and recorded in the He-3 detectors C_2 and C_3.

The experiment [1] was carried out at the interferometry facility of the 10 MW research reactor of the University of Missouri (MURR) in a BARC-Vienna-MURR collaboration. A 2.35 Å polarized neutron beam illuminated a skew symmetric (220) LLL silicon interferometer. Due to the space constraints within the interferometer, the maximum mechanical rotation of each flipper was limited to $\pm 22^\circ$. Larger angles $\delta\beta$ were therefore achieved electrically. A reversal of current in F_1 effectively rotates F_1 through 180°, yielding $\delta\beta = 180^\circ$. A current reversal of F_2 instead results in $\delta\beta = -180^\circ$.

The experimental geometric phases Φ_G are plotted in figure 2. The straight line in the figure represents the theoretical prediction (6). Points for $\delta\beta$ values between -40° and $+40^\circ$ represent mechanical rotations of the flippers. Rotations $\delta\beta = -180^\circ, 180^\circ$ and (the second point at) 0° were produced electrically by reversing the current in F_2, F_1 and both flippers respectively.

Bhandari [24] has opined that plotting geometric phases for mechanical as well as electric rotations of the flippers on the same curve in figure 2 is unjustified, since the two results originate from different parameter spaces. He has also questioned the assignment of a phase magnitude of 180° in figure 2 for a flipper current reversal, since a phase equal to any odd integral multiple of 180° can be obtained by a judicious variation of individual currents in the two coils of a flipper, during the current reversal.

Contrary to Bhandari's contention however, geometric phase is governed solely by the geometry of the curve traced in the ray space, irrespective of the Hamiltonian or the parameter space of the experiment. Regardless of the means adopted for rotating F_1 and F_2, the spinor acquires a geometric phase $\delta\beta$ equal to minus half the solid angle between the two spin curves. Even for an electronically effected [25] rotation $\delta\beta = (\omega_1 - \omega_2)t$ between F_1

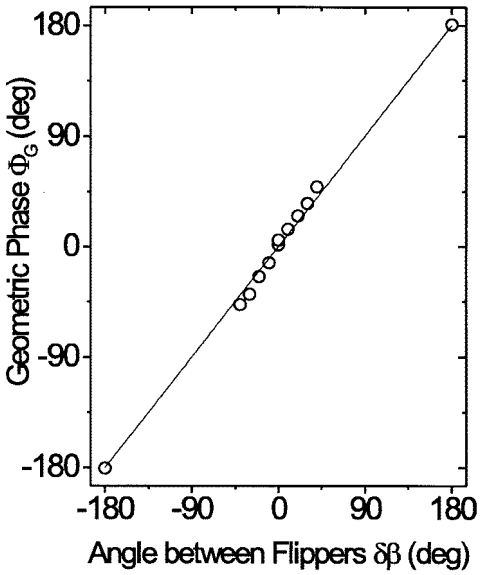

Figure 2. Pure geometric phase Φ_G resulting from a relative rotation $\delta\beta$ between the flippers F_1 and F_2.

and F_2, the corresponding time-proportional geometric phase manifests itself as quantum beats (cf. §6). A current-reversed flipper is indistinguishable to the spinor from a flipper rotated mechanically by $\pm 180^\circ$. The ambiguity in sign was removed in the experiment [1] by assuming that a current reversal produces a counterclockwise, i.e. $+180^\circ$, rotation. Furthermore, two coils of each flipper were connected in series, implying a single current. Geometric phase was observed by reversing the current (*not currents*) in a flipper. For a smooth current variation during the reversal, the spinor evolution (cf. eqs (11a), (11b) and (12) of [4]) exhibits a phase jump equal to just 180° and *not* any higher odd multiple of 180°, as the current changes sign. All data points in figure 2 therefore belong there rightfully.

With the flippers held normal to the respective subbeams ($\delta\beta = 0$) interference patterns were recorded for several translations of F_1 and F_2. Figure 3 displays the variation of the pure dynamical phase with displacement δx of F_1 (for $\delta\beta = 0$). The slope agrees well with that expected (7) for the applied guide field B_0.

5. Verification of Pauli anticommutation

In the experiment [1], each π-flipper was a dual-flipper [4] made of two coils producing π-precessions in succession, about two mutually orthogonal axes, say $\hat{\mathbf{I}}$ and $\hat{\mathbf{II}}$. These axes of precession lie in a vertical plane and subtend angles $+\pi/4$ and $-\pi/4$ respectively with $\hat{\boldsymbol{z}}$. The net operation is given by $\mathrm{e}^{(-i\sigma_{\mathrm{II}}\pi/2)}\mathrm{e}^{(-i\sigma_{\mathrm{I}}\pi/2)} = (-i\sigma_{\mathrm{II}})(-i\sigma_{\mathrm{I}}) = -\sigma_{\mathrm{II}}\sigma_{\mathrm{I}}$. Here σ_{I} and σ_{II} are the components of the Pauli spin operator $\boldsymbol{\sigma}$ along $\hat{\mathbf{I}}$ and $\hat{\mathbf{II}}$ respectively. On reversing the current in the coils, the order of the two fields gets reversed. The

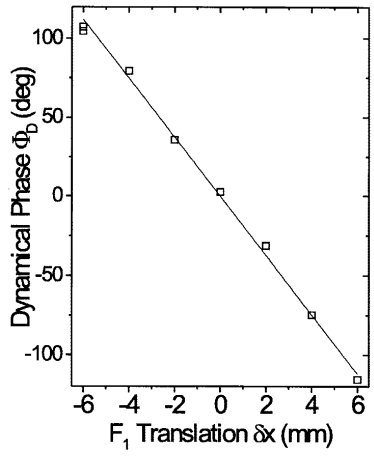

Figure 3. Pure dynamical phase Φ_D as a function of the translation δx of the flipper F_1.

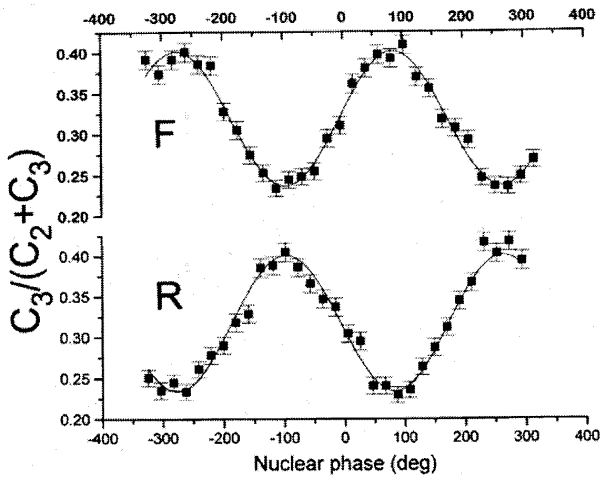

Figure 4. Direct verification of Pauli anticommutation. The interferogram has shifted by $180.5^\circ \pm 3.0^\circ$ on switching the current in the flipper F_1 from the forward (F) sense to the reverse (R) sense.

reversed flipper operates as $e^{(-i\sigma_I \pi/2)} e^{(-i\sigma_{II} \pi/2)} = -\sigma_I \sigma_{II} = \sigma_{II} \sigma_I$, since σ_I and σ_{II} anticommute, being orthogonal components of the Pauli spin operator. The reversed flipper operation thus differs only in sign from the original operation. This sign change manifests as a π phase shift [4,12] of the spinor. This π phase jump can only be observed interferometrically. A polarimetric experiment measures phases only modulo π [19,26] and hence can not sense anticommutation.

Figure 4 depicts the interference patterns recorded with the current in the flipper F_1 switched between the forward (F) and reverse (R) directions. On reversing the current, the

pattern just gets reflected about the line representing its average, as expected. The observed phase shift equals 180° to within 2%, confirming the anticommutivity between $\sigma_{\rm I}$ and $\sigma_{\rm II}$. If the current in F_2 is also reversed, the interferogram shifts further by 180° becoming identical to the initial interferogram.

This experiment constitutes the first direct verification of Pauli anticommutation.

6. Quantum beats: Manifestation of time varying geometric phase

In the quantum beats experiment of Badurek *et al* [25], an incident $|z\rangle$-polarized neutron beam traversed radiofrequency resonant spin flippers in the two arms of the interferometer. A minute frequency difference $\delta\nu = 0.02$ Hz maintained between the two flippers resulted in interference oscillations with a time period of 50 sec. This experiment is a special case of the experiment separating geometric and dynamical phases, described in §4. Here at any instant t, the angle between the two flippers $\delta\beta$ equals $2\pi\delta\nu t$ and produces a pure geometric phase [10,27]. The quantum beats result from the time-proportional part $2\pi\delta\nu t$ of this geometric phase. Thus interpreted by Wagh and Rakhecha, the quantum beats experiment [25] constitutes an early measurement of geometric phase.

7. Polarimetric observation of geometric and dynamical phases

Since Berry discovered geometric phase in adiabatic evolutions [9], the early experimenters implemented adiabatic evolutions and used the '1-Hamiltonian 2-state' strategy (cf. §3) to observe geometric phase. Tomita and Chiao [16] propagated linearly polarized light along a coiled optical fibre and measured the concomitant rotation of the polarization. The rotation equalled Ω, the solid angle spanned by the closed curve traced adiabatically by the optical wave vector on the sphere of directions. This rotation resulted from geometric phases $\mp\Omega$ acquired by the two eigenstates, viz. the right and left circular polarizations. In analogous neutron experiments, polarized neutrons were subjected to a magnetic field completing a revolution *adiabatically* over a cone. Bitter and Dubbers [17] employed a spatial field variation and Richardson *et al* [18], a temporal variation. From the observed rotation of the neutron spin, a small geometric phase $\mp\Omega/2$ for the two eigenstates was discerned from the large dynamical phase characteristic of adiabatic evolutions.

The interferometric experiment described in §4 however takes no recourse to adiabaticity. The neutron polarimetric version [2] of this experiment was carried out at the polarimetry setup on the tangential beam port of the 250 kW *TRIGA* research reactor at the Atominstitut of the Austrian Universities in Vienna. A schematic sketch of the setup is shown in figure 5. Here the incident neutron beam in the $|y\rangle$ state, viz. a superposition of $|z\rangle$ and $|-z\rangle$ states, successively traversed the flippers F_1 and F_2. A uniform guide field $B_0\hat{\mathbf{z}}$ was applied over the setup. Geometric and dynamical phases for $|z\rangle$ state, originating from relative rotations and translations respectively of F_1 and F_2 were measured by observing concomitant spin rotations of the incident $\hat{\mathbf{y}}$ spin. The polarization analysis of the emergent beam yielded the intensity I_{yy} which varies linearly with $\cos 2\Phi$. Two sets of data were recorded, one for identical rotations $\delta\beta/2$ (parallel flippers) and the other with opposite rotations, of the two flippers. 3-D plots of I_{yy} made as a function of the

flipper rotations $\delta\beta/2$ and F_2 translations δx are depicted in figures 6 and 7 for parallel and opposite rotations respectively.

Ideally, one would not expect any variation of the detected intensity for parallel rotation of the flippers, since for a fixed displacement δx, neither the geometric nor the dynamical phase should change. However, if the neutron beam is not centered exactly on the rotation axis of a flipper, the rotation produces a spurious displacement δx of the flipper and a consequent dynamical phase contamination. A beam centre offset of about 1 mm can explain the observed small intensity variation with $\delta\beta$ in the parallel rotation data. For opposite flipper rotations, the intensity varies cosinusoidally with $\delta\beta$, as expected.

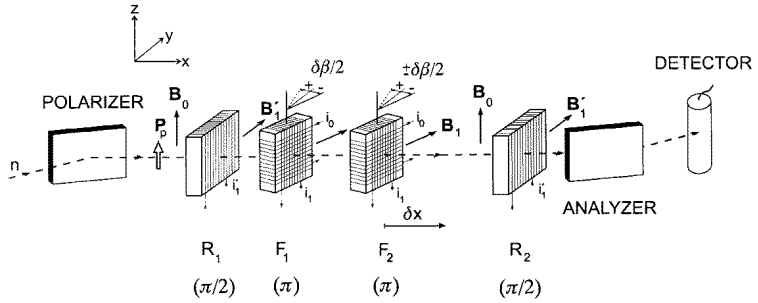

Figure 5. Sketch of the polarimetric experiment to observe demarcated geometric and dynamical phases for the $|z\rangle$ state, arising from relative rotations and translations respectively between F_1 and F_2.

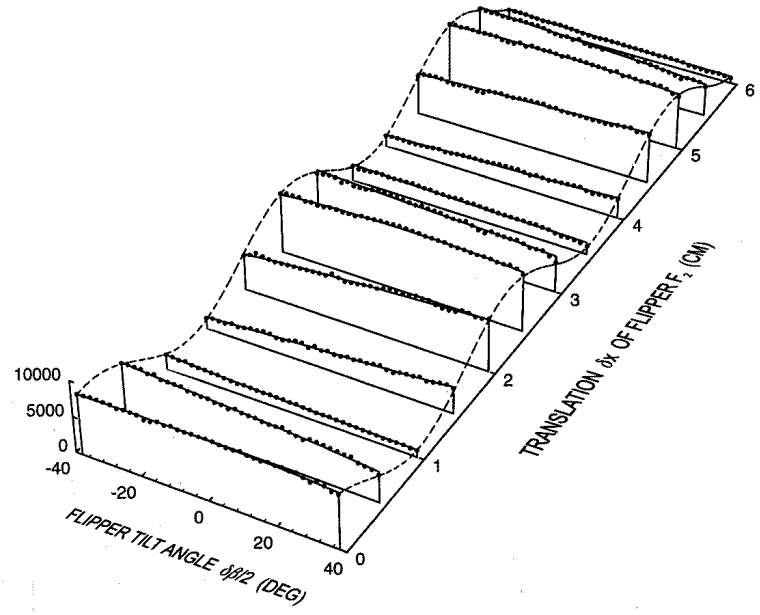

Figure 6. Measured intensity I_{yy} for parallel rotation $\delta\beta/2$ of flippers F_1 and F_2 for a series of downstream displacements δx of the flipper F_2, along with computed fits to data. I_{yy} is practically flat along the $\delta\beta/2$ axis.

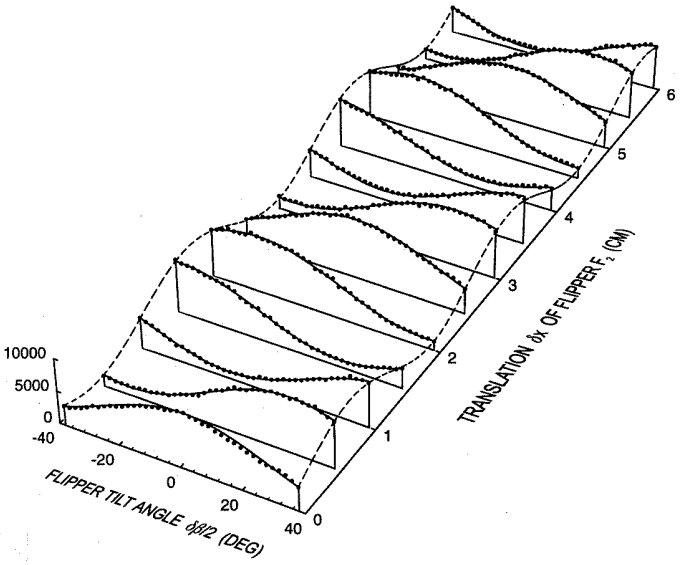

Figure 7. Same as figure 6 but with the two flippers rotating in opposite directions.

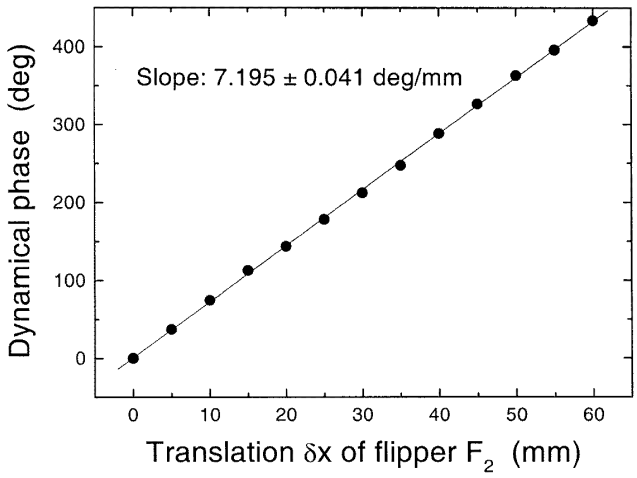

Figure 8. Pure dynamical phase Φ_D as a function of the translation δx of flipper F_2. The straight line is the best fit to the data.

The dynamical phase variation with the translation δx of F_2, derived from the opposite rotation data, is shown in figure 8. The slope of its linear fit is in close agreement with the measured field value.

The geometric phases obtained from the opposite-rotation data, corrected for the dynamical phase contamination, are plotted in figure 9 against the angle between flippers F_1 and F_2. The experiment agrees with theory to within about 1%.

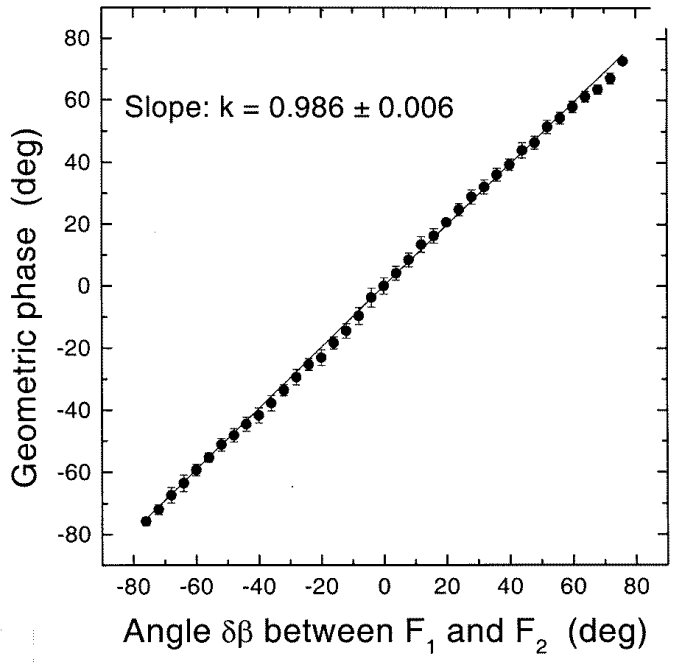

Figure 9. Observed geometric phase as a function of the angle $\delta\beta$ between the flippers F_1 and F_2. The straight line is the best fit to the data.

To eliminate the dynamical phase contamination, the experiment was repeated by placing the flippers within a 'field-free' soft magnetic box [28]. The intensity patterns $I_{yy}(\delta\beta/2)$ recorded for parallel and opposite rotations $\delta\beta/2$ of the flippers F_1 and F_2, are converted to the fractional polarization $P_y(\delta\beta/2)/P_y(0)$ in figure 10. The curve for parallel-rotation remains flat as expected for the null geometric phase, while the opposite-rotation curve oscillates cosinusoidally due to the concomitant geometric phase. The corresponding geometric phases extracted from the raw data for opposite rotations are displayed in figure 10 as a function of the flipper rotations. These phases conform to theory very closely.

8. Phase observation: Polarimetry vis-a-vis interferometry

The polarimetrically observed geometric as well as dynamical phases [2] are within about 1% of theoretical predictions, representing a marked improvement over the agreement level achieved in the interferometric experiment [1]. The improved precision has resulted primarily from the inherent advantages of the neutron polarimetric method. Neutron polarimetry is insensitive to ambient mechanical and thermal disturbances. It is also free from spatial constraints imposed by small perfect crystal interferometers. In an interferometric experiment, the perfect crystal interferometer accepts neutrons incident within an angular range of only a few arcseconds at each neutron wavelength, thus reducing the usable neutron intensity by about 3 orders of magnitude. A polarimetric measurement on the

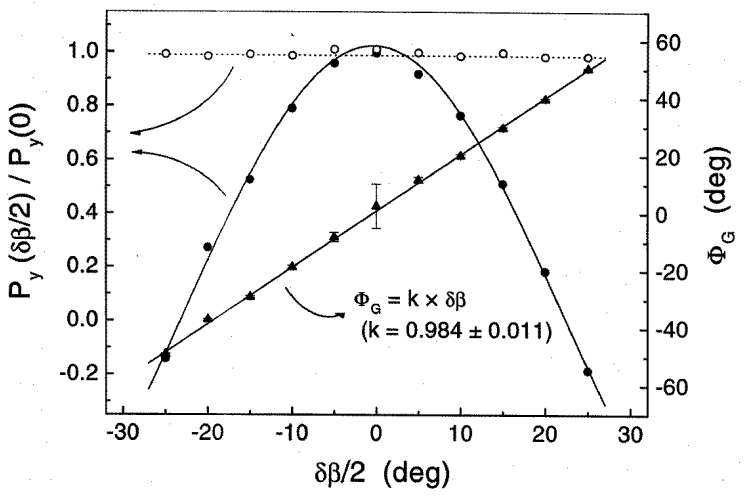

Figure 10. Measured normalized polarization $P_y(\delta\beta/2)/P_y(0)$ for parallel ($\circ$) and opposite ($\bullet$) rotations $\delta\beta/2$ of flippers F_1 and F_2, mounted in a field-free region within a soft magnetic shielding. The phases derived from the parallel- and opposite- (shown by filled triangles) rotation data without applying any corrections conform well to the theoretical geometric phases equal to 0 and $\delta\beta$ respectively. Curves through the data points represent the best fits.

other hand, uses a substantial fraction of the incident neutron intensity and hence can be carried out even at a low-flux reactor. Furthermore, here both the orthogonal states comprised in each neutron acquire identical scalar phases which therefore get eliminated in the resultant spin rotation, providing a clean SU(2) phase measurement. The polarimetric experiment of Badurek *et al* [29] could thus observe scalar Aharanov–Bohm phases with a white neutron beam and establish their nondispersivity. The only limitation of a polarimetric experiment is its modulo 180° phase measurement, since the two orthogonal states acquire equal and opposite SU(2) phases Φ and $-\Phi$. This is the reason why Pauli anticommutation can not be verified polarimetrically.

9. Observation of noncyclic phases and amplitudes

In a noncyclic evolution, the phase (2) is accompanied by a noncyclicity-dependent interference amplitude (3), as prescribed by the Pancharatnam connection. In an interferometric experiment, the phase and amplitude are measured from the *shift* and *attenuation* respectively of the interference pattern relative to that recorded for a reference cyclic evolution. Noncyclic phases and amplitudes can also be measured in a suitably devised polarimetric [26] experiment.

In the first experiment [3] observing noncyclic phases and amplitudes, the neutron spin underwent a precession ϕ_L about a static magnetic field at an angle θ. The associated phase Φ and interference amplitude $\mathcal{A}$ for this unitary evolution are given by eqs ((2), (3))

$$\mathcal{A} = \sqrt{1 - \sin^2\theta \sin^2\frac{\phi_L}{2}} = \cos\frac{G}{2} = \sqrt{\frac{1 + \mathbf{s}_i \cdot \mathbf{s}_f}{2}} \leq 1, \tag{8}$$

$$\tan\Phi = -\tan\frac{\phi_L}{2}\ \cos\theta. \tag{9}$$

Here G is the length of the shorter geodesic between the initial and final spins $\mathbf{s}_i$ and $\mathbf{s}_f$ respectively. The dynamical phase [10]

$$\Phi_D = \int \frac{\mu \mathbf{s} \cdot \mathbf{B} \mathrm{d}t}{\hbar} = -\frac{\phi_L}{2}\cos\theta\,, \tag{10}$$

is proportional to the integral of the component of the magnetic field along the spin direction (cf. eq. (4)) and the geometric phase [10,19]

$$\Phi_G = \Phi - \Phi_D = -\frac{\Omega}{2}, \tag{11}$$

Ω denoting the solid angle subtended at the centre of spin sphere by the closed curve on the spin sphere obtained by joining the ends of the arc traced by $\mathbf{s}$ on the θ-cone with the shorter ($G < \pi$) geodesic.

The interference oscillations for this noncyclic evolution, viz.

$$\mathcal{I}(\chi, \theta, \phi_L) \propto D + \mathcal{A}\cos(\chi + \Phi)\,, \tag{12}$$

are shifted by $-\Phi$ and attenuated by a factor $\mathcal{A}$ relative to the reference pattern

$$\mathcal{I}(\chi, \theta, \phi_L = 0) \propto D + \cos\chi\,, \tag{13}$$

both recorded with an auxiliary scalar phase χ.

Figure 11 depicts the experiment schematically. The experiment was performed at the V9 interferometry setup [30] in the Berlin Neutron Scattering Center (BENSC) of the Hahn-Meitner-Institut, Germany, employing a 2 Å polarized neutron beam. A guide field along the vertical ($\hat{\mathbf{z}}$) was applied over the entire setup (about 45 G in the interferometer region).

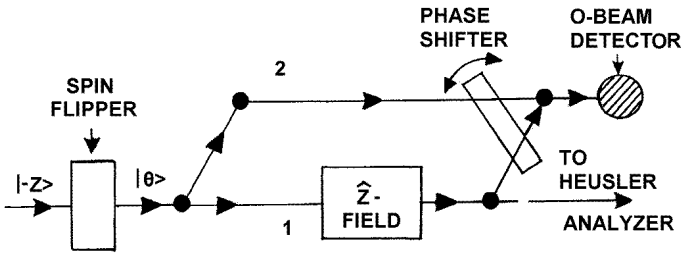

Figure 11. Experimental arrangement (schematic). A magnetic guide field is applied along $\hat{\mathbf{z}}$, transverse to the plane of the diagram. The spin of the monochromatic neutrons incident on the interferometer makes an angle θ with $\hat{\mathbf{z}}$. An O-beam interference pattern is obtained by rotating the phase shifter for a given additional $\hat{\mathbf{z}}$-field introduced on path **1** of the skew symmetric interferometer.

The spin of the polarized neutron beam illuminating the interferometer (figure 11) could be set at any desired angle θ to the guide field along $\hat{\mathbf{z}}$ and any desired precession ϕ_L of the neutron spin $\mathbf{s}$ on a cone of polar angle θ about $\hat{\mathbf{z}}$ could be obtained by introducing an additional field with a $\hat{\mathbf{z}}$-field gadget in path $\mathbf{1}$ of the interferometer.

The experiment [3] involved 5 spinor states in all, characterized by incident spin angles $\theta = 0°$, $70.5°$, $90°$, $109.5°$ and $180°$. In each run, two interference patterns were simultaneously recorded one for the evolution (θ, ϕ_L) of interest and the other for a reference evolution (θ_R, ϕ_{LR}), say. The pattern pairs belonged to two categories: θ-pairs for fixed ϕ_L and ϕ_L-pairs for fixed θ. The relative phase difference and amplitude ratio between the evolution of interest (θ, ϕ_L) and the reference evolution (θ_R, ϕ_{LR}), could hence be determined unambiguously.

The phases and amplitudes for four θ pairs corrected for incomplete polarization of incident beam are depicted against ϕ_L in figures 12 and 13 respectively.

The phase difference between $\theta = 0°$ and $\theta_R = 180°$ states just equals $-\phi_L$. The phase differences for θ angles $70.5°$, $90°$ and $109.5°$ reproduce the predicted nonlinear relations as a function of the precession ϕ_L. For a given θ, $\mathcal{A}$ has a minimum (figure 13) equal to $|\cos\theta|$ at $\phi_L = \pm 180°$, where the angle G between the spin vector precessing over the θ-cone and the initial spin vector reaches its maximum, viz. 2θ. The reduction of the interference contrast near $\phi_L = \pm 180°$, seen in figure 13 and the lower pattern of figure 14, lowers the precision of phase determination and causes relatively large error bars on the measured phase shifts (figures 12 and 14) for $\theta = 70.5°$, $90°$ and $109.5°$.

For $\theta = 90°$, the spin traverses along the equator of spin sphere, spanning the angle $G = \phi_L$. The dynamical phase vanishes identically since the spin is orthogonal to the

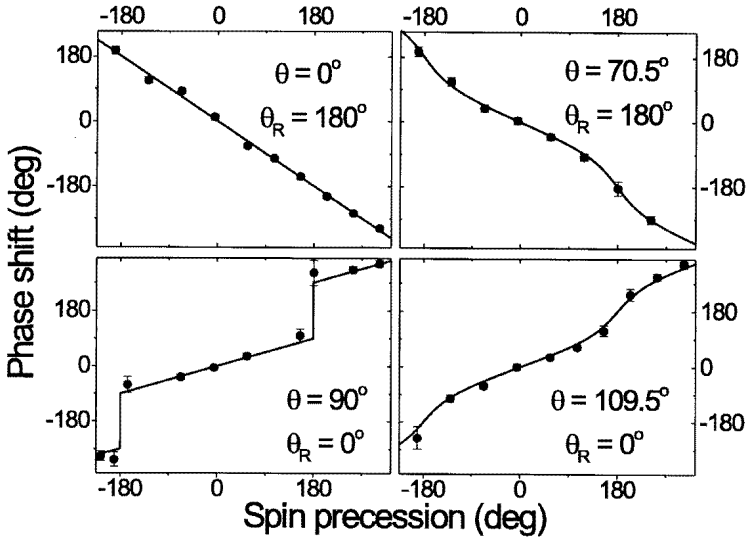

Figure 12. Corrected phase shifts between incident states with spin angles θ and θ_R as a function of the precession ϕ_L. Solid curves represent the theoretical phases. Note large error bars for noncyclic evolutions near $\phi_L = \pm 180°$ due to the reduced interference amplitude (cf. figure 13).

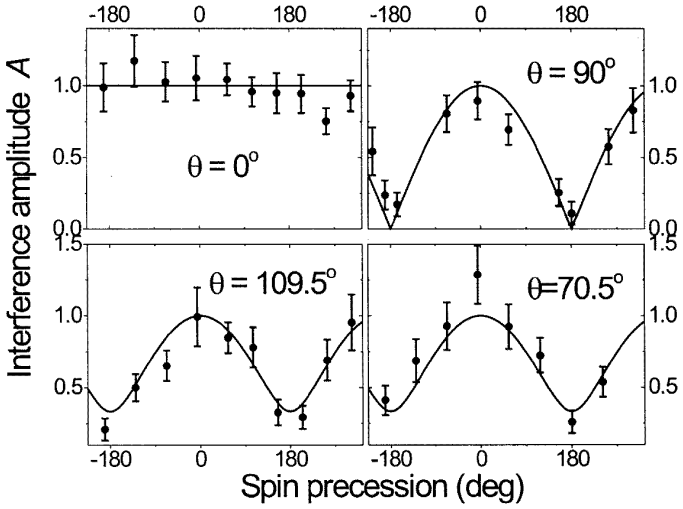

Figure 13. Corrected interference amplitudes for 4 incident spin angles θ. The smooth curves are the theoretical predictions.

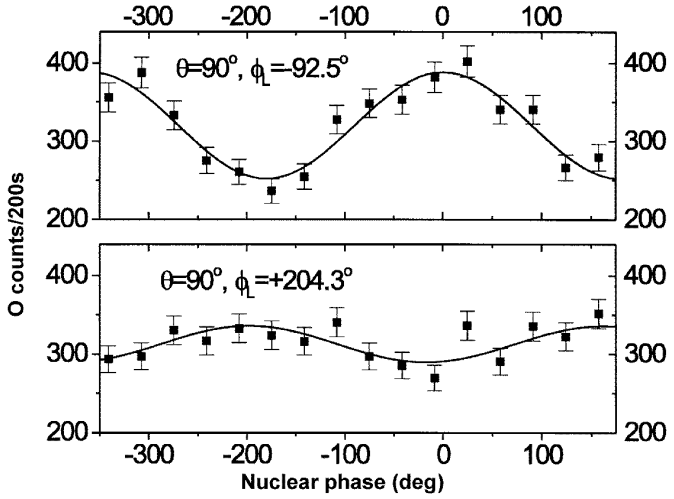

Figure 14. Interference patterns recorded with $I = 1.2$ and -1.2 A in the $\hat{\mathbf{z}}$-field gadget for $\theta = 90^\circ$, display a phase shift $197^\circ \pm 17^\circ$ against the expected 180° phase jump occurring across $\phi_L = 180^\circ$. The smooth curves are the best sinusoidal fits.

field (eq. (4)). The phase and amplitude are now determined by $\mathcal{A}e^{i\Phi} = \cos(\phi_L/2)$ which is real and changes sign across odd integral values of $\phi_L(\mathrm{deg})/180$. This corresponds to an amplitude $\mathcal{A} = |\cos(\phi_L/2)|$ (figure 13) and a staircase function [13], of 180° high and 360° long steps, for the phase Φ. For $-180^\circ < \phi_L < 180^\circ$, the geodesic traversed is

shorter than π and the shorter geodesic between its ends just retraces it. Hence the closed curve encloses no solid angle and yields a null geometric phase (eq. (5)). The total phase acquired by the $\theta = 90^\circ$ state over this ϕ_L range is hence zero. At $\phi_L = -180^\circ$ or 180°, an infinite number of geodesics, each of length π, can be drawn between the ends $-\mathbf{s}_i$ and $\mathbf{s}_i$ of the traversed arc, rendering Ω, Φ_G and hence Φ indeterminate. Here the initial and final states of the evolution being mutually orthogonal ($\mathcal{A} = 0$), do not interfere. When ϕ_L crosses -180° or 180°, the shorter geodesic closing the arc lies on the other side and completes the equator, enclosing a hemisphere ($\Omega = \pm 2\pi$) to yield a $\mp 180^\circ$ jump [1,22] in $\Phi = \Phi_G$. This phase jump manifests itself as a shift between the interferogram pair (figure 14) for $\theta = 90^\circ$ recorded with $\hat{\mathbf{z}}$-field gadget currents $I = 1.2$ and -1.2 A ($\phi_L = 204.3^\circ$ and -92.5° respectively). The difference between the staircase phase for $\theta = 90^\circ$ and the phase $-\phi_L/2$ for $\theta_R = 0^\circ$ climbs a sloped step function (figure 12), as verified in this experiment.

Thus over the θ domain, we have one extreme, viz. $\theta = 0^\circ$ or 180° of cyclic evolutions yielding unattenuated interferograms ($\mathcal{A} = 1$) with dynamical phases $-\phi_L/2$ or $\phi_L/2$ respectively. In the other extreme of $\theta = 90^\circ$, the interference pattern just gets modulated by $\cos(\phi_L/2)$, implying an attenuation $\mathcal{A} = |\cos(\phi_L/2)|$ and geometric phase jumps of 180°.

The values $\mathcal{A}\cos\Phi$ computed from the observations for $\theta = 0^\circ$, 70.5°, 90°, and 109.5° are plotted in figure 15. As expected [13], they all lie close to the single curve representing $\cos(\phi_L/2)$, the quantity that would be observed if the intensity oscillations are recorded as a function of ϕ_L, without employing a scalar phase χ. The product $\mathcal{A}\cos\Phi$ therefore is independent of θ though $\mathcal{A}$ and Φ depend individually on θ. Figures 12, 13 and 15 conclusively dispel widely prevalent misconceptions (cf. e.g. [31–33]) about the noncyclic phase.

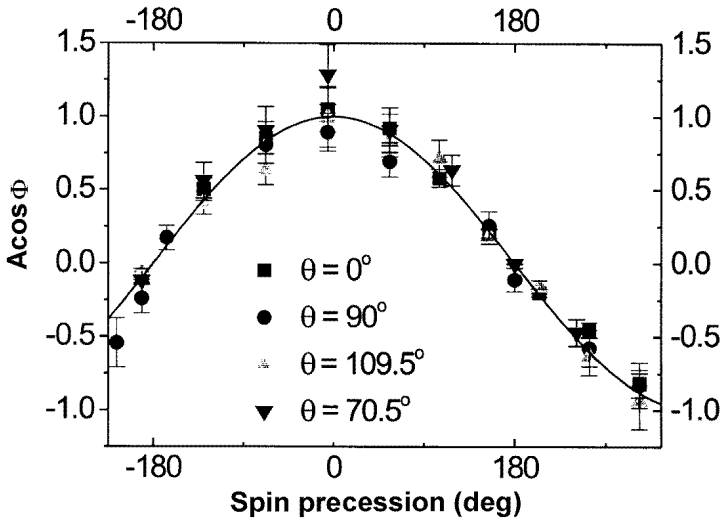

Figure 15. The products of the observed interference amplitudes and cosines of the corresponding phases for 4 incident angles θ, all lie close to the single curve $\cos(\phi_L/2)$.

Bhandari [24] contends that this experiment [3] measured not the noncyclic phase itself, but the *difference* between phases for the θ and θ_R states and hence failed to verify the different sign of the phase for states in the upper and lower spin hemispheres. He also objects to the 'arbitrary' choice made in the experiment for the sign of the phase jump observed for $\theta = 90^\circ$.

Contrary to Bhandari's claim, the experiment [3] did determine the sign of Φ/ϕ_L unambiguously for each of the five θ spinors studied, from the interference pattern pairs $(\theta, \phi_L)-(\theta, \phi_{LR})$. One pattern pair for each θ corresponded to $\phi_{LR} = 0^\circ$, yielding the *noncyclic phase itself*. Phase shifts derived from 14 such pattern pairs were included in the data set subjected to a comprehensive least squares fit (cf. right column on p. 1993 in [3]). A pattern pair of this kind recorded for $\theta = 90^\circ$ is depicted in figure 14.

Like most interference experiments, the experiment [3] could measure phases only modulo 360°. The consequent ambiguity about the sign of the 180° phase jumps observed for $\theta = 90^\circ$ (figure 12) was removed by assigning them the $+$ sign, i.e. treating 90° as the limit taken from the obtuse angle side. The limit of the phase shift curve for $\theta_R = 0^\circ$ taken by varying θ smoothly from 180° through 109.5° to 90° thus coincides with the 90° curve.

Bhandari's criticism [24] of the experiment [3] is therefore not correct.

To conclude, the first observation [3] of interference amplitudes and phases in noncyclic evolutions has elucidated the physics underlying the Pancharatnam connection [6] in its entirety.

10. Acknowledgements

It is a pleasure to thank coauthors of papers [1–3] for fruitful collaboration. Financial support from and use of neutron facilities in Atominstitut, Vienna, Austria, University of Missouri-Columbia, USA and Berlin Neutron Scattering Center (BENSC) at Hahn-Meitner-Institut, Germany are gratefully acknowledged.

References

[1] A G Wagh, V C Rakhecha, J Summhammer, G Badurek, H Weinfurter, B E Allman, H Kaiser, K Hamacher, D L Jacobson and S A Werner, *Phys. Rev. Lett.* **78**, 755 (1997); *J Phys. Soc. Jpn. Suppl.* **A65**, 73 (1996)
[2] A G Wagh, G Badurek, V C Rakhecha, R J Buchelt and A Schricker, *Phys. Lett.* **A268**, 209 (2000)
[3] A G Wagh, V C Rakhecha, P Fischer and A Ioffe, *Phys. Rev. Lett.* **81**, 1992 (1998); **83**, 2090 (1999)
[4] A G Wagh, *Phys. Lett.* **A146**, 369 (1990)
[5] A G Wagh and V C Rakhecha, *Pramana – J. Phys.* **41**, L479 (1993)
[6] S Pancharatnam, *Proc. Indian Acad. Sci.* **A44**, 247 (1956)
[7] M V Berry, *J. Mod. Optics* **34**, 1401 (1987)
[8] A G Wagh and V C Rakhecha, *J. Phys.* **A32**, 5167 (1999)
[9] M V Berry, *Proc. R. Soc. London* **A392**, 45 (1984)
[10] A G Wagh and V C Rakhecha, *Phys. Lett.* **A148**, 17 (1990)
[11] A G Wagh and V C Rakhecha, *Phys. Rev.* **A48**, R1729 (1993)
[12] A G Wagh, *Ind. J. Pure Appl. Phys.* **33**, 566 (1995)

[13] A G Wagh and V C Rakhecha, *Phys. Lett.* **A197**, 107 (1995)
[14] A Shapere and F Wilczek (eds), *Geometric phases in physics* (World Scientific, Singapore, 1989)
[15] M Berry, *Phys. Today* **43**, 12, 34 (1990)
[16] A Tomita and R Chiao, *Phys. Rev. Lett.* **57**, 937 (1986)
[17] T Bitter and B Dubbers, *Phys. Rev. Lett.* **59**, 251 (1987)
[18] D J Richardson, A I Kilvington, K Green and S K Lamoreaux, *Phys. Rev. Lett.* **61**, 2030 (1988)
[19] A G Wagh and V C Rakhecha, *Phys. Lett.* **A170**, 71 (1992)
[20] H Rauch, W Treimer and U Bonse, *Phys. Lett.* **A47**, 369 (1974)
[21] G Badurek, H Rauch and A Zeilinger (eds), Matter Wave Interferometry, *Physica* **B151** (1988)
[22] A G Wagh and V C Rakhecha, *Prog. Part. Nucl. Phys.* **37**, 485 (1996)
[23] V C Rakhecha and A G Wagh, *Pramana – J. Phys.* **46**, 315 (1996)
[24] R Bhandari, *Pramana – J. Phys.* **56**, 000 (2001)
[25] G Badurek, H Rauch and D Tuppinger, *Phys. Rev.* **A34**, 2600 (1986)
[26] A G Wagh and V C Rakhecha, *Phys. Lett.* **A197**, 112 (1995)
[27] A G Wagh and V C Rakhecha, in *Recent developments in quantum optics* edited by R Inguva (Plenum Press, New York, 1993) p. 117
[28] G Badurek, *J. Phys. Soc. Jpn.* (*Suppl.*) **A65**, 60 (1996)
[29] G Badurek, H Weinfurter, R Gähler, A Kollmar, S Wehinger and A Zeilinger, *Phys. Rev. Lett.* **71**, 307 (1993)
[30] G Drabkin, A Ioffe, S Kirsanov, F Mezei and V Zabijakin, *Nucl. Inst. Meth.* **A348**, 198 (1994)
[31] H Weinfurter and G Badurek, *Phys. Rev. Lett.* **64**, 1318 (1990)
[32] R C Casella and S A Werner, *Phys. Rev. Lett.* **69**, 1625 (1992)
[33] R C Casella, *Phys. Rev. Lett.* **73**, 2941 (1994)